Spatiotemporal dynamics of traction forces show three contraction centers in migratory neurons

Jian Jiang,[1,2] Zheng-hong Zhang,[1] Xiao-bin Yuan,[1] and Mu-ming Poo[1]

[1]Institute of Neuroscience, State Key Laboratory of Neuroscience, CAS Center for Excellence in Brain Science, Shanghai Institutes for Biological Sciences, Chinese Academy of Sciences, Shanghai, China 200031
[2]Graduate School of the Chinese Academy of Sciences, Shanghai, China 200031

Traction force against the substrate is required for neuronal migration, but how it is generated and regulated remains controversial. Using traction force microscopy, we showed in cultured granule cells the coexistence of three distinct contraction centers (CCs) that are located at the distal and proximal regions of the leading process as well as at the trailing process, regions exhibiting high-level myosin-II activities. The CC activities depended on myosin-II, actin filaments, and microtubules, as well as substrate adhesion, and exhibited apparently independent fluctuation. The difference of strain energies associated with CC activities between leading versus trailing processes tightly correlated with the displacement of the soma at any given time. Application of brain-derived neurotrophic factor (BDNF) and Slit2, factors known to guide neuronal migration, at the leading process altered CC activities by regulating the small GTPases Cdc42 and RhoA, respectively, leading to forward and rearward soma translocation. These results delineate the multiple origins and spatiotemporal dynamics of the traction force underlying neuronal migration.

Introduction

Migration of neurons from their birthplace to the designated areas is a critical step in the development of brain architecture (Hatten, 1999; Ayala et al., 2007). This migration is believed to be a directed process, in which guidance cues in the developing brain regulate neuronal contractile activities that drive neuronal migration. Much progress has been made in our understanding of the cellular and molecular basis of neuronal migration in vitro (Solecki et al., 2009) and in vivo (Tsai et al., 2007), including the role of various cytoskeleton contractile components (He et al., 2010), their regulation by intracellular signaling pathways (Feng and Walsh, 2001), and transduction mechanisms underlying cellular responses to extracellular guidance cues (Wu et al., 1999; Guan et al., 2007). However, the biomechanical aspects of neuronal migration are only beginning to be explored (Moore and Sheetz, 2011).

Mechanical forces generated by cells or tissues play important roles in a variety of biological processes, such as sensing of substrate rigidity (Plotnikov et al., 2012), assembly of focal adhesion (Balaban et al., 2001; Roca-Cusachs et al., 2013), cell fate determination (Yim and Sheetz, 2012), cell polarization (Houk et al., 2012), directional cell migration (Weber et al., 2012), epithelial spreading (Behrndt et al., 2012), and wound healing (Brugués et al., 2014). At the cellular level, traction force measurements showed that a single contraction center (CC; or "dipole") is responsible for generating the traction force for fibroblast migration (De et al., 2007). And there is also a comprehensive model suggesting that the anterior region, soma, and posterior region play different roles in fibroblast migration (Guo and Wang, 2012). Unlike fibroblasts, the soma of migrating neurons is much smaller in size and extends long leading processes (LPs) and trailing processes (TPs) that may translocate relatively independently with respect to the soma, suggesting that the spatiotemporal pattern of traction force generation in migrating neurons may be substantially different from that of the fibroblast. At the subcellular level, actin filaments (F-actin) and the associated nonmuscle myosin-II are responsible for the contractile activity and migration of many cell types (Vicente-Manzanares et al., 2009). A high concentration of myosin-II has been found at the leading growth cone (He et al., 2010), proximal region of the leading process (pLP; Solecki et al., 2009), or TP (Martini and Valdeolmillos, 2010). By examining the relationship between myosin-II distribution and soma translocation, the main indicator of neuronal migration, previous studies have proposed disparate models of

Correspondence to Mu-ming Poo: mpoo@ion.ac.cn

Z.-h. Zhang's present address is Dept. of Neurology, Dongfeng Hospital, Hubei University of Medicine, Hubei, China.

X.-b. Yuan's present address is Hussman Institute for Autism, Baltimore, MD 21201.

Abbreviations used in this paper: BDNF, brain-derived neurotrophic factor; CC, contraction center; dLP, distal region of the leading process; GC, granule cell; LP, leading process; MT, microtubule; P, postnatal day; PAA, polyacrylamide; pLP, proximal region of the leading process; TIRF, total internal reflection fluorescence; TFM, traction force microscopy; TP, trailing process.

The Rockefeller University Press $30.00
J. Cell Biol. Vol. 209 No. 5 759–774
www.jcb.org/cgi/doi/10.1083/jcb.201410068

force generation that drive soma translocation: the soma may be pulled by the proximal region of the LP (pLPs; Solecki et al., 2009) or the growth cone of the LP (He et al., 2010), or pushed by the TP (Martini and Valdeolmillos, 2010). In addition, there is evidence that microtubules (MTs) may also be involved in regulating neuronal migration, as suggested by the finding that MT depolymerization induced by pharmacological agents or down-regulation of the motor protein kinesin-5 by RNA interference could accelerate neuron migration (He et al., 2010; Falnikar et al., 2011). In the present study, we first found that traction force may be generated simultaneously at up to three different regions in migrating neurons, including the distal region of the LP (dLP), pLP, and TP. We then performed quantitative analysis of the spatiotemporal dynamics of force generation at these three CCs, and further investigated the role of various cytoskeletal components and adhesions in the force generation.

Neuronal migration during development is regulated by guidance cues (Ayala et al., 2007), which act on the growing tip of neuritic processes at distant locations from the soma (Guan et al., 2007). The neurotrophin brain-derived neurotrophic factor (BDNF) exerts both chemokinetic (Borghesani et al., 2002) and chemotactic (Yuan et al., 2003) effects on cultured neurons (Park and Poo, 2013). Genetic depletion of BDNF impairs the migration of granule cells (GCs) to the molecular zone of developing mouse cerebellum (Borghesani et al., 2002). In developing mouse telencephalon, Slit1/2 repels neuronal precursor cells migrating from the anterior subventricular zone to the olfactory bulb (Wu et al., 1999). Frontal application of Slit2 to the LP of cultured cerebellar GCs also induces growth cone collapse and reverses the direction of GC migration (Guan et al., 2007). The long neuritic processes of migration neurons and the existence of directional sensing mechanisms at the neuritic growth cone suggest that traction forces generated at different regions of the neuron must be properly coordinated in order to achieve effective neuronal migration.

Among many methods for measuring mechanical properties of cells or tissues, only traction force microscopy (TFM; Munevar et al., 2001) and stress-sensitive biosensors (Grashoff et al., 2010) can be used to measure the traction force of the entire cell. Two commonly used cell substrates for TFM are nanopillars (du Roure et al., 2005) and polymer sheets embedded with microbeads (Munevar et al., 2001). Fluorescent microbead-loaded polyacrylamide (PAA) gel substrate could be prepared with various degrees of stiffness suitable for studying different cell types, e.g., fibroblasts (Munevar et al., 2001), epithelial cells (Serra-Picamal et al., 2012), and neurons (Chan and Odde, 2008), by setting the PPA concentration. This method allowed us to measure neuronal traction forces that were found in this study to be much weaker than those generated by fibroblasts (Butler et al., 2002) or glial cells. By monitoring the displacement of microbeads over prolonged periods around the entire neuron, we have identified up to three distinct CCs coexisting in the same neuron, and further examined spatiotemporal dynamics during spontaneous migration and under the influence of guidance factors. Our results provide a comprehensive description of the spatiotemporal dynamics of contractile activities and their regulation by guidance molecules in migrating neurons, as well as the underlying cytoskeletal and molecular mechanisms.

Results

Three CCs identified by TFM

Cerebellum GCs were obtained by dissociating cerebella of newborn rats on postnatal day 0–2 (P0–P2) and cultured on the PAA substrate embedded with fluorescent microbeads (see Materials and methods). We measured the displacements of discrete beads in the surrounding substratum with time, relative to their substrate locations in the absence of the cells, as determined after cell removal with osmotic lysis at the end of time-lapse imaging (Fig. 1 a). There is no observable displacements of beads at a distance beyond ∼30 µm from the cell (Fig. 1 b), indicating that bead displacements around the neuron reflect the deformation of the PAA gel caused by neuron-generated traction force rather than osmotic lysis. We then transformed the displacement vectors (Fig. 1 a_3) into a continuous map of displacements (Fig. 1 a_4, see Materials and methods) and stress (Fig. 1 c_1, see Materials and methods).

We found that the stress map is highly dynamic, exhibiting large variations with time at different regions around the cell (Video 1). For example, the relatively dark area shown in Fig. 1 c_1 at the dLP behind the growth cone was a CC location at the time of observation, as indicated by convergent stress vectors. However, within minutes, two additional CCs at pLP (Fig. 1 c_2) and TP (Fig. 1 c_3) were observed in the same cell. Moreover, coexistence of two CCs with similar contractile activities was often observed, as illustrated in another cell in Fig. 1 c_4. In GCs with more than two primary neurites, we had observed the existence of dominant CCs at all neurites at the same or different times, as illustrated in the example cell in Fig. S1, d–f. For GCs with a bifurcating LP, each branch had an independent CC (Fig. 1 c_5). Since GCs with bifurcating processes or more than two primary processes were relatively rare, we focused only on nonbifurcating bipolar GCs in the present study. In 72 cells examined, we found that 9, 32, and 31 cells exhibited 3, 2, and 1 dominant CCs, respectively, at the three different regions (dLP, pLP, and TP) during the ∼40-min observation period (Fig. 1 e_4 and Tables S1 and S2). Thus, by identifying the sites of convergent stress vectors, we have consistently identified three locations where the CC appears most in migrating GCs, sometimes with multiple CCs simultaneously active. The CCs can also be visualized by representing the stress field in a 3D color map or a "pinwheel" color map in which directions of stress vectors are represented by color (Fig. S1, a–c).

To fully characterize the spatiotemporal dynamics of traction forces, we determined the CC location automatically by calculating the maximal change of stress directions between two adjacent points on the cell axis (darkest region in the Fig. 1 d, marked by green dots) with time over the observation period. As shown in Fig. 1 d, relative to the center of mass of the soma, the CC location moved up and down along the neuronal axis with time. Multipeak Gaussian fitting of the cumulated frequency of the locations of dominant CC along the axis showed three distinct peaks at dLP, pLP, and TP, consistent with the three CC locations identified by convergent stress vectors (see Fig. S2 for other examples).

The stress detected in the substrate represents the resultant action of contractile activities of all CCs. The activity at one CC may be dominant so that the activities of other CCs are not clearly observed by microbead displacements in the substrate. However, the activity of nondominant CCs could be revealed by measuring the changes in stress (displacement) vectors with

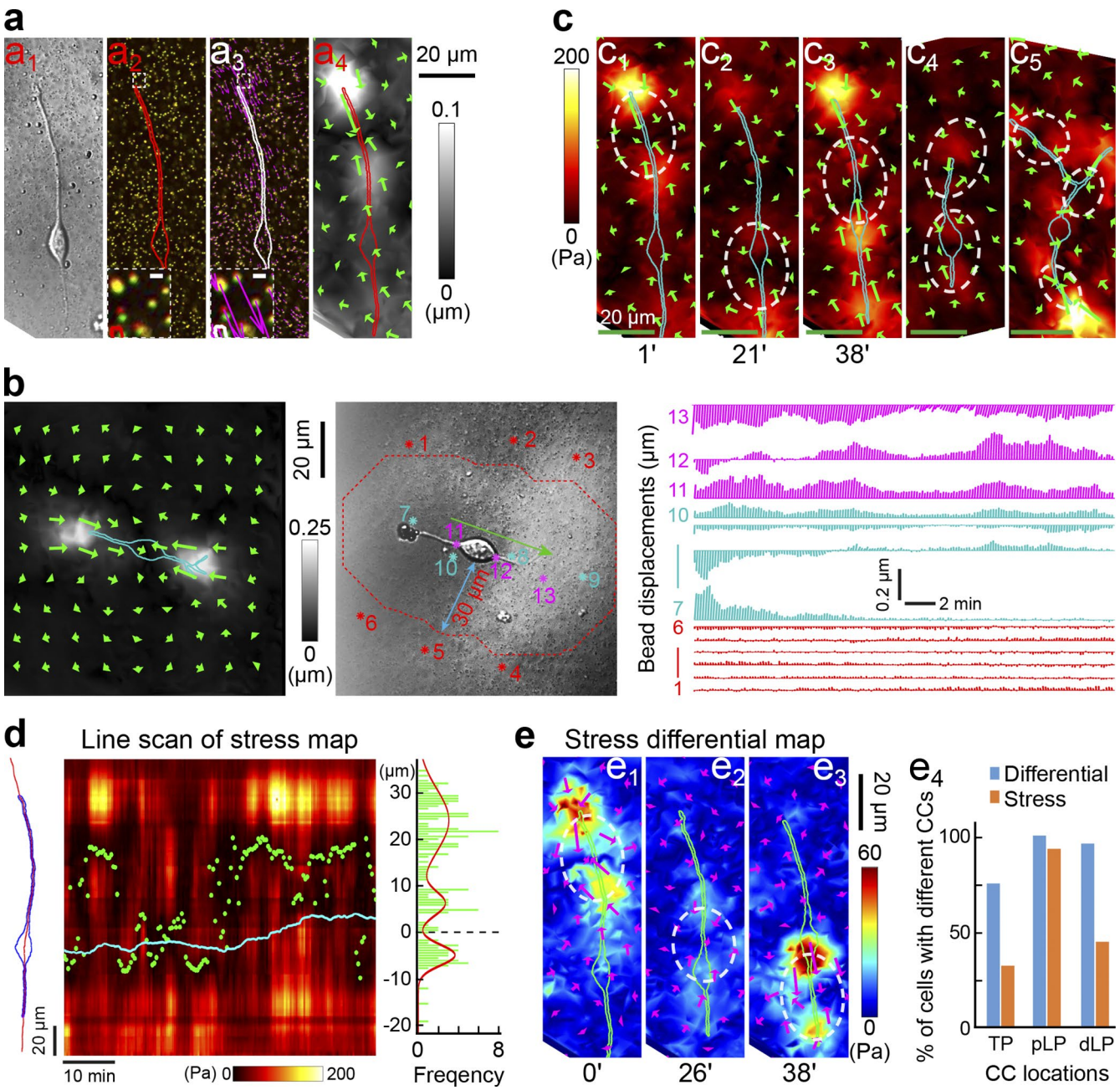

Figure 1. **Three CCs identified by TFM.** (a) Steps in determining microbead displacements around a GC. a_1, image of a GC. a_2, superimposed image of fluorescent beads before (red) and after (green) osmotic lysis of the cell. Insets show the boxed regions at a higher resolution (bars, 1 μm). Solid traces, cell outline. a_3, discrete displacement vectors, with arrow length and arrowheads representing displacement magnitude and direction, respectively. a_4, continuous displacement field map (coded in grayscale) obtained by interpolation of discrete displacement vectors in a_3, marked by regularly spaced vectors. (b) Displacement of the bead at different distances from the GC. (b, left) Displacement map. (b, middle) Beads close to (cyan and purple asterisks, <30 μm) and distant from (red asterisks, ≥30 μm) the neuron. Green arrow, direction of soma translocation. Broken line, points ≥30 μm away. (b, right) Changes of displacements with time for beads at different distances. No displacement was observed for distant beads (red). (c) Stress maps of substrates. c_1–c_3, stress maps computed from the continuous displacement field maps at different times for the same GC shown in a, and three distinct CCs (white circles) were observed at three different times. c_1, stress map at t = 1 min (the same time as in a). c_2, t = 21 min. c_3, t = 38 min. c_4, stress map caused by another GC showing two coexisting CCs. c_5, each bifurcating process generated its own CC. (d) CC locations identified by a stress map generated by the same typical GC shown in a. (d, left) Outline (blue) and axis (red) of the GC. (d, middle) Dynamics of the stress along the axis of the migratory GC at different distances from the tip of the TP over a 60-min period, obtained from the stress map similar to that shown in c_1. Line bins, 21 s. The location of the CCs (marked by green dots), determined as the site of the maximal absolute value of the angular difference between stress vectors of adjacent pixels (see Materials and methods). Cyan line, soma center. (d, right) Frequency distribution of CCs observed at different distances away from the soma during the observation period for the cell shown on the left. Red curve, best fit with a multi-peak Gaussian function (R = 0.61). Broken black line, soma center. Additionally, 18 more cases are shown in Fig. S2 and a total number of 72 GCs are summarized in e_4. (e) CC locations identified by a stress differential map. e_1–e_3, changes in the stress ("stress differential," ΔF over Δt = 21 s) at three different time points (t = 0, 26, and 38 min) for the same cell as in a, with ΔF color-coded. Note that three different CCs were identified (broken lines) as regions with convergent stress differential vectors. e_4, percentage of cells showing CCs at three different locations. dLP, distal end of LP; pLP, proximal end of LP; TP, trailing process. Histograms, data from all 72 GCs, each for an ~40-min observation period, with the CC location determined by stress map (orange) and stress differential map (blue).

time at different locations, i.e., the stress differential (ΔF within Δt = ∼10–21 s). As shown in Fig. 1, e_1–e_3, by calculating the changes of local stress over the previous 21-s period, we found a significant stress differential occurring at three CCs locating at dLP, pLP, and TP at three different times, as indicated by the region with convergent vectors of stress differentials. (CCs can also be identified as regions with divergent stress differentials that reflect the reduction of CC contractile activity, see Fig. 3). By using a stress differential map, we found that all 72 cells examined had at least two distinct CCs, and 51/72 had three CCs. This is more than was found using the stress map alone, as indicated by the histograms in Fig. 1 e_4 and Tables S1 and S2. Therefore, we conclude that migratory GCs have three independent CCs, with the dominant CC shifting among the three with time.

Most previous reports have identified by indirect methods one cellular location for force generation that drives soma translocation: in front of the soma (Solecki et al., 2009), at the growth cone of the LP (He et al., 2010), or at the rear end of the soma (Martini and Valdeolmillos, 2010). Our TFM measurements indicate that contractile activities at these previously identified locations could coexist in the same neuron at the same time.

The absence of "pushing" force in migrating GCs

A common question concerning the mechanism of neuronal migration is whether the soma is pulled by the LP in the front or pushed by the TP at the rear. In the above analysis, we defined CCs as the converging sites of stress (displacement) vectors in the substrate surrounding the neuron. We have specifically searched for sites with divergent stress vectors that would indicate the pushing force generated by the neuron, in particular at the TP, where the pushing force was proposed to cause forward soma translocation (Tsai et al., 2007; Martini and Valdeolmillos, 2010). In all GCs we have examined in this study, we failed to observe any neuron exhibiting divergent stress vectors, and TP of migrating neurons consistently showed only converging stress vectors, as illustrated in Fig. 2 c.

Dynamic CC activity underlies saltatory soma translocation

To assay the temporal dynamics of CC activities in different neuronal regions, we calculated the total regional strain energy (Butler et al., 2002), which better reflects the total instantaneous contractile energy (force times distance) spent by the cell in exerting traction force on the surrounding substrate (see Materials and methods). The total strain energies at three regions—dLP, pLP, and TP—were found to change either synchronously or asynchronously (Fig. 2 a). The existence of asynchrony indicates that contractile activities of different CCs could occur independently. We also found that the contractile activities of glial cells are much larger than that of GCs (Fig. S4, a–c).

We next explored the relationship between soma translocation and CC activities, as reflected by regional strain energies. In the example of migrating neuron in Fig. 2 b, the location of the dominant CC (marked by green dots in the stress map) fluctuated between CCs at dLP and TP, but persisted at dLP when the soma underwent rapid forward translocation, accompanied by a marked increase in the strain energy at dLP. Fig. 2 (c and d) showed that rapid rearward and forward soma translocation occurred when the dominant CC was found at the TP and pLP, respectively. Consistent with the expectation that soma translocation is determined by the net traction force generated by all three CCs on the soma, we found that the magnitude and direction of soma translocation depended directly on the difference of strain energies produced in the LPs versus TPs. Very little migration was observed when the summation of strain energies at dLP and pLP ($S_{dLP} + S_{pLP}$) was similar to that of the TP (S_{TP}; see gray bar in Fig. 2). Roughly, forward and rearward translocation was observed when $S_{dLP} + S_{pLP}$ became larger or smaller than S_{TP}, respectively (see the black bar in Fig. 2). Thus, the net force generated by the contractile activities in the front and rear of the soma determines the direction and magnitude of soma translocation.

Temporally correlated fluctuations of CC activity and soma translocation

To further examine the notion that the net force generated by LP and TP drives the soma translocation, we analyzed the correlation between "instantaneous" soma translocation and stress or stress differential (ΔF over Δt = 15 s) at a higher temporal resolution. In the example GC in Fig. 3, the cell underwent a net forward soma translocation over a period of 42 min, during which there were apparent random fluctuations in the location of the dominant CC as well as forward versus rearward soma translocation (Fig. 3 a, left). However, over a short time segment of ∼5 min (Fig. 3, a and b, green box), the stress (Fig. 3 c) and stress differential (Fig. 3 d) were highly correlated with the direction and magnitude of the soma translocation (Fig. 3 b). Higher stress at dLP (Fig. 3 c, black bar) and TP (Fig. 3 c, gray bar) was observed during forward and rearward soma translocation, respectively (Fig. 3 c). Stress differentials further showed an increase (converging vector toward CC, solid line in Fig. 3 d) and decrease (divergent vectors away from CC, broken line in Fig. 3 d) in the corresponding CC activity during the forward and rearward soma translocation, respectively (boxes below in Fig. 3 d). Further analysis of the temporal cross-correlation for all 28 migrating cells examined in this study between the velocity of soma translocation and strain energies in the LP and TP showed that the soma velocity vector positively correlated with $S_{dLP} + S_{pLP}$ or S_{TP} as well as $S_{dLP} + S_{pLP} - S_{TP}$ (Fig. 2 e). More cases were shown in Fig. S3. Thus, we concluded that soma translocation is determined by the net force generated by the CCs at LP and TP, and fluctuations of CC activities accounts for the apparent saltatory soma translocation at a given time.

Roles of myosin-II and cytoskeletal filaments in force generation

To understand the subcellular mechanism underlying CC activities during neuronal migration, we examined traction force generation under various pharmacological treatments that may affect contractile activity in these neurons. Non-muscle myosin-II is a key molecule for cell migration (Vicente-Manzanares et al., 2009), and its enrichment in pLP has been observed in cerebellar neurons (Solecki et al., 2009). We found that the total strain energy produced by the GC was markedly decreased (by ∼65%; Fig. 4, a and g) by adding 50 µM of myosin-II inhibitor blebbistatin (Bleb) in the culture medium, but markedly elevated (by sixfold) by similar treatment with 2.5 nM myosin-II activator calyculin A (CalyA; Fig. 4, b and g). The distribution of active myosin-II in these neurons cultured on laminin-coated glass substrate was also examined by immunostaining with the antibody against phosphorylated myosin-II light chain. We found that active myosin-II was concentrated mainly in the soma and at distal tips of both LPs and TPs (Fig. 4 h). Fitting of the total

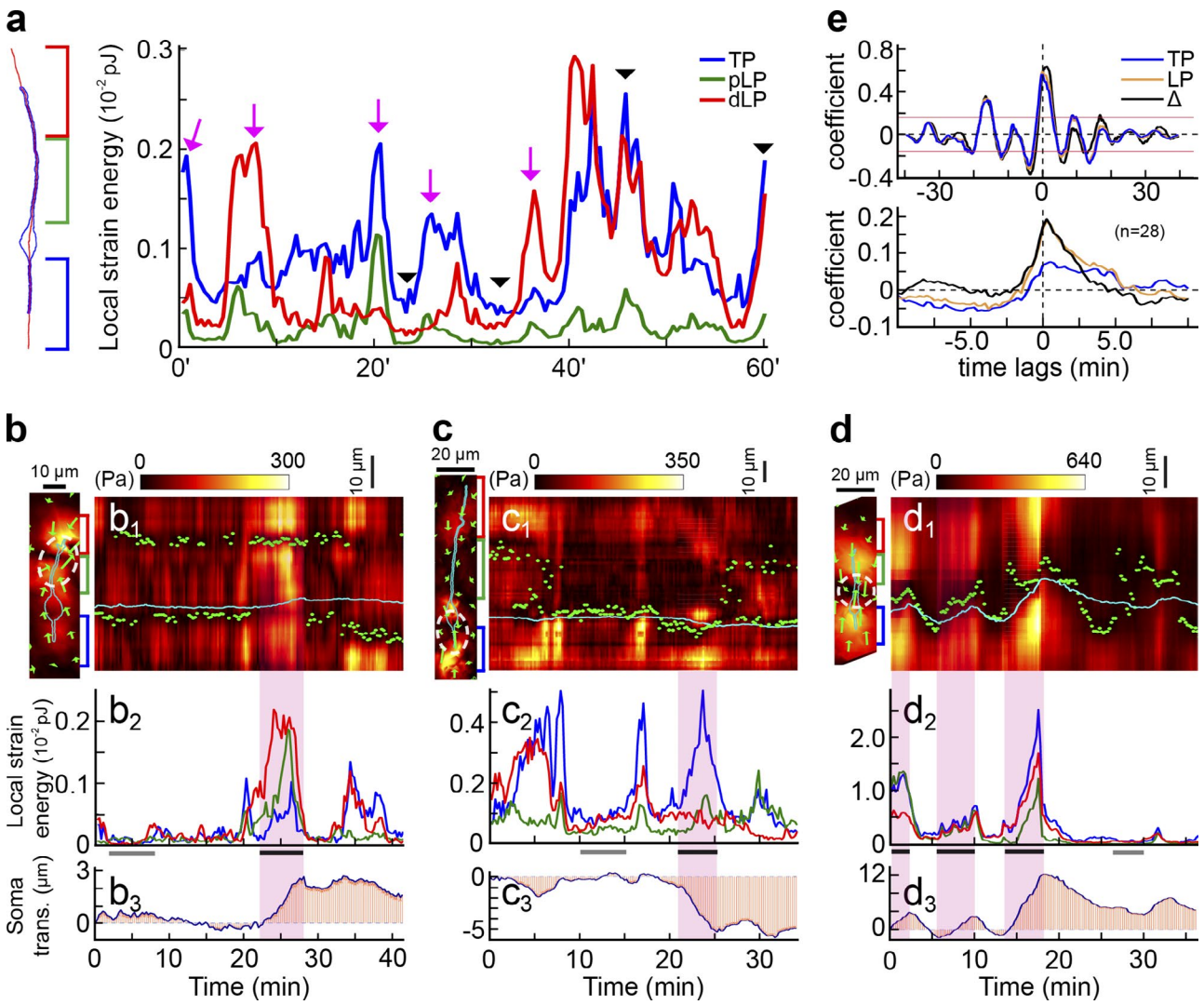

Figure 2. **Dynamic contraction activities at multiple CCs can drive soma translocation.** (a, left) The typical neuron is divided into three regions (marked by colored brackets) roughly corresponding to regions around three CCs: dLP (red), pLP (green), and TP (blue). (a, right) Changes in the total local strain energy (see Materials and methods) of three regions of the GC shown on the left during a 60-min observation period. Arrows, asynchronous contraction of two or three CCs; arrowheads, synchronous contraction of three CCs. Additionally, three more cases are shown in b–d. The dynamic and asynchronous contraction can also be observed in the 18 cases in Fig. S2. (b) CC at dLP pulled the soma forward in a migrating GC. (b, top) Line scan of stress along the cell axis during the observation time. Cyan line, soma center; green dots, position of the dominant CC. (b, middle) Local strain energies at dLP, pLP, and TP. (b, bottom) Soma translocation with time. Pink shade, CC activities at dLP pulled the soma forward. (c and d) Two other migrating GCs showing rapid soma translocation when CC activities at TP and pLP were high, respectively, and strain energies at LP ($S_{dLP} + S_{pLP}$) versus TP (S_{TP}) were highly unbalanced (black bar vs. gray bar). More detailed analysis of five cases similar to b–d are shown in Fig. 3 and Fig. S3, and a total number of 28 GCs were summarized in e. (e) Cross-correlation of the velocity of soma translocation with [$S_{dLP} + S_{pLP}$] (marked as "LP"), S_{TP} ("TP"), and [($S_{dLP} + S_{pLP}$) − S_{TP}] ("Δ"). (e, top) Cross-correlation coefficient for the example cell in d. Red horizontal lines represent the approximate upper and lower confidence bounds (95%), assuming that migration velocity and traction energy are completely uncorrelated. (e, bottom) Averaged cross-correlation coefficient for all 28 migrating cells examined.

immunofluorescence intensity along the neuron with a multi-peak Gaussian function showed three peaks (Fig. 4, i and j) corresponding roughly to the location of the three CCs found in GCs cultured on PAA gel (Fig. 1, d and e_4), except that higher immunostaining was found in the soma but not in the pLP. This may be attributed to the larger cellular volume at the soma.

The role of F-actin in force generation was also examined by applying pharmacological treatments that affect F-actin polymerization and stability. We found that the strain energy produced by the GC was greatly reduced (by ~75%) after treatment with the F-actin depolymerizing drug latrunculin A (LA; 1 μM, Fig. 4, c and g). In contrast, treatment with the F-actin stabilizing drug jasplakinolide (Jasp; 250 nM, Fig. 4, d and g) resulted in stabilization of strain energy production with very little fluctuation around the same average level (Fig. 4, c and g). These results are consistent with the expectation that actomyosin contractility is the main contributor to force generation and further suggest that F-actin dynamics are required for the dynamic fluctuation of force generation.

During cell division, polymerization and depolymerization of MTs provide the pushing and pulling forces, respectively, for chromosome separation (Dogterom et al., 2005). In cultured GCs, however, we found that disrupting MTs by nocodazole (Noc; 0.5 μM) that depolymerizes MTs resulted in an enhanced stress generation (Fig. 4 e) and elevated strain energy (by approximately sixfold; Fig. 4 g), whereas treatment with

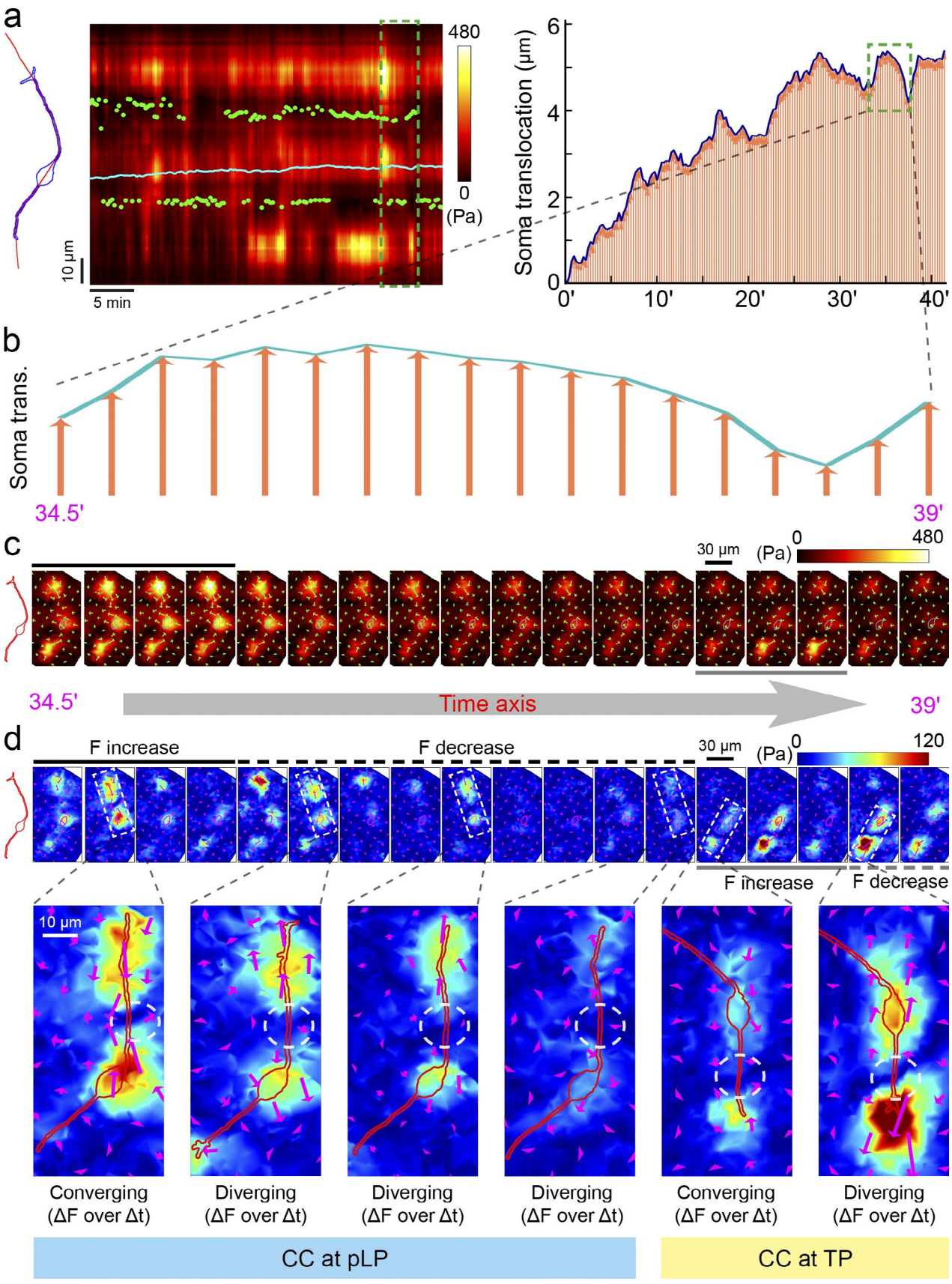

Figure 3. **Temporal correlation between fluctuations in CC activity and soma translocation.** (a) Line scan of the stress along the typical GC axis (left) and soma translocation (right) with time for the same migrating GC. Green dot, location of the dominant CC; cyan line, soma center. Additionally, four more cases were shown in Fig. S3, and a total number of 28 migrating GCs were summarized in Fig. 2 e. (b) Soma displacements during the boxed period in a.

taxol at a concentration (50 nM) known to stabilize MTs (Xiao et al., 2006) produced no obvious effect in the stress (Fig. 4 f) and strain energy (Fig. 4 g). Interestingly, in the presence of myosin-II inhibitor, the elevated strain energy caused by nocodazole was totally abolished and reduced to a level below that found before the treatment (Fig. 4 g), which indicates that the enhanced traction force caused by MT depolymerization depends on myosin-II activity, which is consistent with that found in nonneuronal cells (Rape et al., 2011). Thus, MT dynamics could also regulate traction force generation in neurons.

The role of substrate adhesion in neuronal migration and force generation

The focal adhesion mechanically links the ECM with the termini of F-actin bundles (Patla et al., 2010) and is necessary for the generation of traction force against the substrate. Like most motile cells, neurons migrate in stereotyped steps: leading edge extension, nuclear translocation, and TP retraction. For fruitful forward migration, there must be net forward movement of the soma and TP. This suggests that the degree of substrate adhesion of the LP is larger than that of the soma and TP. We tested this notion by pushing the middle of the LP with a micropipette and determined which part of the neuron become detached from the substrate (Fig. 5 a). This assay showed that in 17/25 of migrating GCs, the soma was the first to be detached from the substrate (Fig. 5 b), demonstrating that substrate adhesion at the distal half of LP is stronger during migration. In contrast, in stationary neurons, the adhesion of soma and TP is stronger than the distal LP (14/16; Fig. 5 b). Thus, net forward migration appears to depend on an increased adhesion at the LP to a level above that of the soma and TP.

FAK is a crucial signaling component of the cell adhesion complex. It can be activated by numerous stimuli and serves as a biosensor or integrator to control cell motility (Mitra et al., 2005). We found that inhibition of FAK kinase activity by the specific drug Y11 (50–200 µM; Golubovskaya et al., 2012) enhanced the strain energy generated by cerebellar GCs (Fig. 5 d). This is consistent with that found in fibroblasts (Rape et al., 2011). The enhancing effect may be attributed to the stabilization of focal contacts via inhibition of their turnover by FAK inhibition (Webb et al., 2004). Alternatively, FAK inhibition can also enhance MT depolymerization (Kaverina et al., 1998; Palazzo et al., 2004) and elevate the RhoA activity(Mitra et al., 2005), which can facilitate myosin-II activation (Kimura et al., 1996), drive actin assembly (Burridge and Wittchen, 2013), and promote growth cone adhesion (Woo and Gomez, 2006). Further studies using total internal reflection fluorescence (TIRF) imaging of immunostained adhesion proteins FAK, paxillin, and vinculin (Fig. 5 c) showed that, unlike the typical clustered focal adhesions found in glial cells (Fig. S4 d), these proteins appeared to be more diffusely distributed in GCs (Fig. 5 c). Similarly, immunostaining of α-actinin and phalloidin-stained F-action showed that stress fibers are less prominent in GCs than in glial cells and fibroblasts (Fig. S4, e and f). Previous studies have also shown that most highly migratory cells lack stress fibers, and the presence of stress fibers is correlated more with strong adhesion than rapid migration (Burridge and Wittchen, 2013).

BDNF and Slit2 regulate traction force and guide neuron migration

In developing cerebellum, BDNF secreted by the Purkinje cell layer is necessary for GCs to migrate across the molecular layer (Borghesani et al., 2002; Poblete-Naredo et al., 2011). We found that local perfusion of BDNF (0.5 µg/ml) to the tips of processes steers the soma translocation in these cultured GCs toward the site of BDNF application. As shown in the example cell in Fig. 6 a, BDNF application enhanced forward soma translocation when applied at a dLP, but reversed soma translocation when applied at a TP. Measurements of the changes of soma translocation velocity, either positive (forward) or negative (rearward), showed that BDNF application at the longer process of the cell (12/21 leading and 9/21 trailing) resulted in an overall positive increase in the velocity (Fig. 6 a, right, n = 21). A previous study has shown that application of Slit-2 at the dLP of these cultured GCs resulted in the reversal of soma translocation (Guan et al., 2007). Given these guidance effects of BDNF and Slit-2 on soma translocation, we further inquired whether the action of the two guidance factors is mediated by regulating CC activities in these GCs.

When BDNF was bath applied to the culture medium, we found that force generation by the entire neuron was markedly enhanced (Fig. 6 b) and the total strain energy of the cell was increased (by up to fourfold; Fig. 6 c). As shown by the example cell in Fig. 6 d, we found that local perfusion of BDNF to dLP resulted in a local increase in the stress. A forward shift in the location of dominant CC (green line) was accompanied by a gradual forward soma translocation (cyan line). The summary of results from all nine GCs examined showed significant forward CC shifts after BDNF application at dLP (Fig. 6 d, right).

BDNF activates Cdc42 (Sieg et al., 2000; Yuan et al., 2003; Myers et al., 2012), a member of the Rho family of small GTPases, which further activates myosin-II via MRCK (Gomes et al., 2005; Wilkinson et al., 2005), promotes F-actin polymerization by the N-WASP–Arp2/3 pathway (Carlier et al., 1999), and enhances point–contacts dynamics (Myers and Gomez, 2011; Matsuda et al., 2012; Myers et al., 2012), all of which can enhance the contractile activity of the cell. We found that when BDNF was applied together with the Cdc42 inhibitor ML141 (10–20 µM), the enhancement of force generation induced by BDNF was markedly reduced (Fig. 6 c). Such a result supports the idea that the BDNF effect on force generation is mediated by Cdc42.

Previous studies have shown that frontal application of Slit2 to migrating GCs reversed the front-to-end distribution of RhoA and led to the reversal of neuronal migration in vitro (Guan et al., 2007). RhoA is a small GTPase and can facilitate myosin-II activation by inhibiting myosin phosphatase (Kimura et al., 1996); drives actin assembly by stimulating myosin activity, inhibition of cofilin-mediated F-actin severing, and ac-

(c) Stress during the period marked by the box in a. Black line, period of forward soma translocation, when the contractile activity of the CC at LP was higher; gray line, rearward soma translocation when the contractile activity of the CC at the TP was higher. (d) Stress differential representing the change in the stress (ΔF over Δt = 15 s) for the same period as in c. Boxed areas are shown at a higher spatial resolution below. White circles, the region with the highest change in the direction of stress differential, indicating CC location. Note the increase and decrease of stress differential (ΔF over 15 s) at a dominant CC at pLP, followed by another dominant CC at TP. Red lines, cell outline.

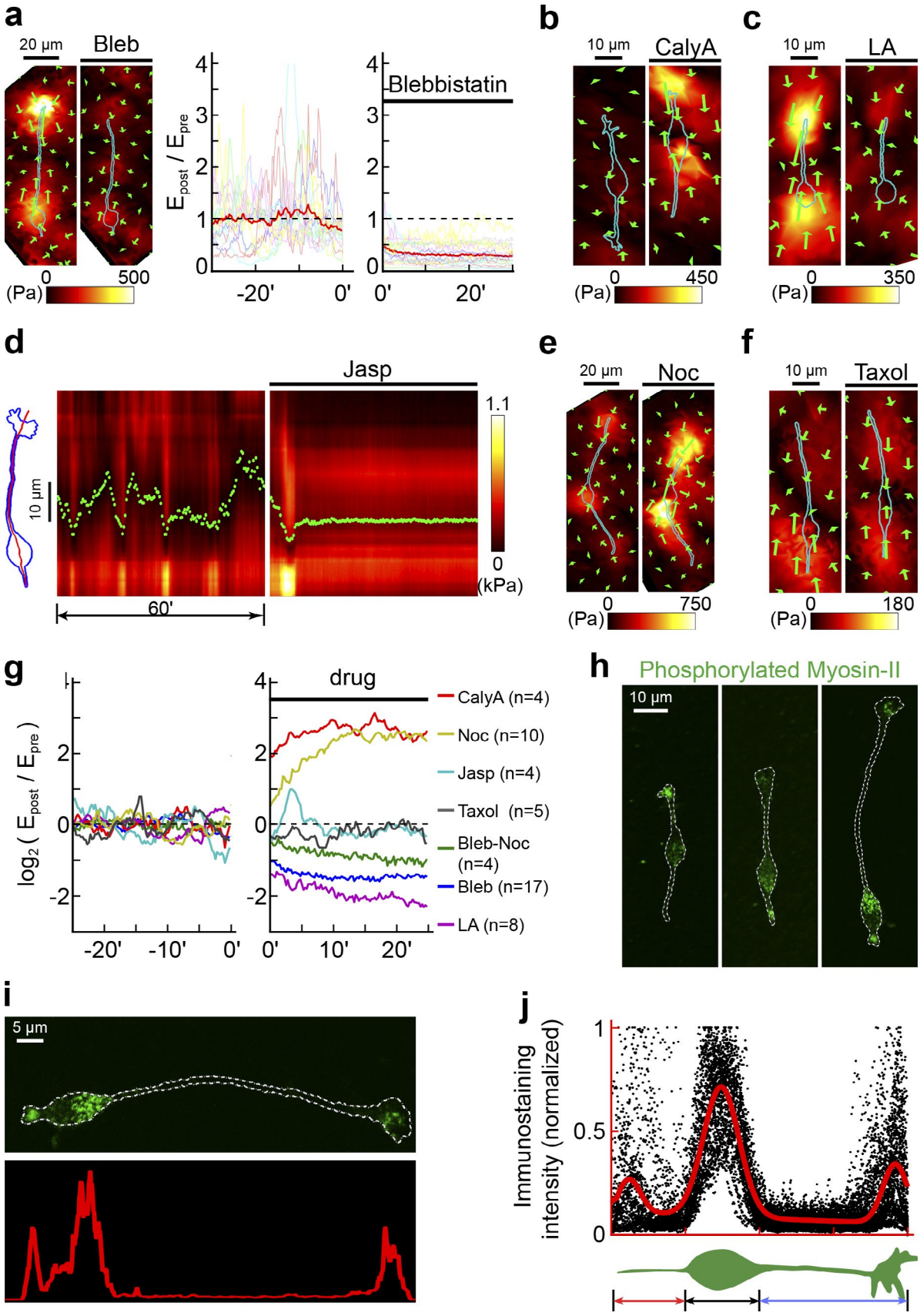

Figure 4. **The roles of myosin-II, actin filaments, and MTs in the contractile activity of GCs.** (a, left) The stress field generated by a GC before and after treatment with the myosin-II inhibitor blebbistatin (Bleb, 50 μM, black line). (a, right) Total strain energy generated by GCs before and after Bleb treatment, with the red thick trace representing the average of 17 cells (individual traces in faint colors). Before averaging, data from each cell were normalized by

tivation of mDia driving actin polymerization (Burridge and Wittchen, 2013); and promotes the formation and stabilization of growth cone point contacts (Woo and Gomez, 2006). In our study, we found that bath-applied Slit2 (0.5 µg/ml) caused the collapse and retraction of GC growth cones. The total strain energy of the cell was largely unchanged after retraction (Fig. 6 c), indicating that Slit2 had not altered the overall level of contractility in GCs. When Slit2 (5 µg/ml) was applied locally to the LP growth cone, we found an initial increase of the stress in pLP followed by an increase in the TP (Fig. 6 e). Concurrently, the position of dominant CC shifted from dLP to TP (Fig. 6 e), accompanied by the reversal of soma translocation. Summary of results from all 10 cells analyzed showed significant rearward shifts of the dominant CC after exposure to Slit2 at dLP (Fig. 6 e). Finally, inhibition of RhoA by Y27632 decreased the total strain energy by ∼50% (Fig. 6 c). These findings of RhoA's contribution in force generation and LP-to-TP shift of the dominant CCs are consistent with the previous report (Guan et al., 2007) that frontal application of Slit2 reverses the distribution of RhoA toward TP. Thus, Slit2 reverses neuron migration by reversing the location of the dominant CC through a process mediated by RhoA.

Discussion

This study of spatiotemporal dynamics of traction forces in migrating GCs using TFM led to three major findings (Fig. 7). First, three distinct and independently fluctuating CCs exist in each GC, and the net action of CC activity drives soma translocation. Second, both F-actin and MTs contribute to the traction force generation, through myosin-II–dependent processes. Third, the attractive and repulsive guidance cues, BDNF and Slit2, respectively, exert their influence on GC migration by altering spatiotemporal dynamics of CC activities at LPs and TPs. To our knowledge, this was the first demonstration of coexistence of multiple CCs and their dynamic regulation during neuronal migration. These results resolved the previous controversy over the location of force generation that drives neuronal migration, and showed that CC-generated pulling rather than pushing is responsible for soma translocation.

The role of cytoskeletons in traction force generation

Although MTs represent the main cytoskeleton conferring the stiffness of the neuron (Spedden et al., 2012) and bearing the compressive load (Brangwynne et al., 2006), they also play an important regulatory role in cellular force generation. Consistent with the previous finding in migrating fibroblast (Rape et al., 2011), we found that in migrating neurons nocodazole-induced depolymerization of MTs enhanced the traction force, whereas inhibition of depolymerization by taxol had no detectable effect. It's also consistent with our laboratory's previous report that local perfusion of nocodazole in the LP can accelerate the neuron migration (He et al., 2010). Furthermore, the inhibition of myosin-II activity by blebbistatin abolished the traction force increase caused by nocodazole. The fact that MT depolymerization enhances traction force may be because its shortening can activate RhoA by releasing GEF-H1 (Waterman-Storer and Salmon, 1999; Kaverina and Straube, 2011; Akhshi et al., 2014) and help to stabilize cell adhesions (Akhshi et al., 2014). Via the MT binding proteins, there is a balance between the amounts of F-actin and MTs. Increasing F-actin is accompanied by decreasing MTs (Even-Ram et al., 2007), and MTs decreasing can increase the amounts of F-actin (Even-Ram et al., 2007). MTs can also promote changes at specific regions of the actomyosin cortex, and in turn the actomyosin cortex influences MT stability (Akhshi et al., 2014). Thus, although myosin-II–dependent actomyosin contractility provides the main source of traction force during neuronal migration, MT dynamics could also have a modulatory effect.

Other contractile activities affecting traction force generation

Besides the contraction of actomyosin, other factors such as the molecular clutch (Oakes and Gardel, 2014) and cortical actin (Salbreux et al., 2012) may also play important roles in generating the traction force. Stress generated within the cytoskeleton drives the retrograde flow of F-actin. Although engagement of focal adhesions results in a reduction of actin retrograde flow rates around adhesion sites and an increase in traction stresses (Gardel et al., 2008), the "clutch engagement" at a focal adhesion can increase the density and affinity of the binding between F-actin and ECM (Oakes and Gardel, 2014). As a cross-linked actin network beneath cell membrane, the cortical actin can generate tension by myosin activity and F-actin cross-linking (Salbreux et al., 2012). When the cortical tension is not uniform throughout the cell, contractility gradients can result in local contraction, as exemplified by the cell body retraction during lamellipodial cell migration and leading edge protrusion in amoeboid motion (Salbreux et al., 2012).

The role of substrate adhesion in migration and force generation

Cell adhesion is necessary for the generation of the traction force against the substrate. Although cell adhesion does not actively generate forces, they mediate force transmission between the cytoskeleton and ECM. The asymmetry of adhesion strength found in our study (Fig. 5) may be caused by the asymmetric distribution of surface adhesion molecules or differential binding affinity between these molecules with their ECM ligands. Among various adhesion molecules, the integrin family is the best known and plays a prominent role in cell migration (Parsons et al., 2010). The binding affinity of integrins can be regulated by an inside-out signaling pathway that includes many intracellular activators (Shattil et al., 2010;

the mean value before the drug treatment (E_{pre}). (b–c and e–f) Stress maps for typical neurons before and after treatment with calyculin A (CalyA; 2.5 nM), latrunculin A (LA; 1 µM), nocodazole (noc; 0.5 µM), and taxol (50 nM), respectively. (d) Line scan of the stress produced by a neuron over a 1-h duration before and after jasplakinolide treatment (jasp; 0.25 µM). (g) Changes in total strain energy (logarithmic scale, base 2) induced by seven different drugs. Each curve represents average of data from many cells (number shown) normalized before averaging. (h) Distribution of activated (phosphorylated, "p") myosin-II (green) in three typical neurons, immunostained for phosphorylated myosin-II light chain. Note that active myosin-II is concentrated near the three CCs. White line, cell outline. (i) Quantitative assay of the p-myosin-II distribution in GCs. Immunostaining intensity of the cell along the axis of the neuron was measured and plotted. (j) Red curve represents best fit of the p-myosin-II distribution with a multi-peak Gaussian function ($R = 0.78$, $n = 37$). The data from each cell were normalized by the highest intensity observed as well as by the length of LP, soma, and TP, respectively.

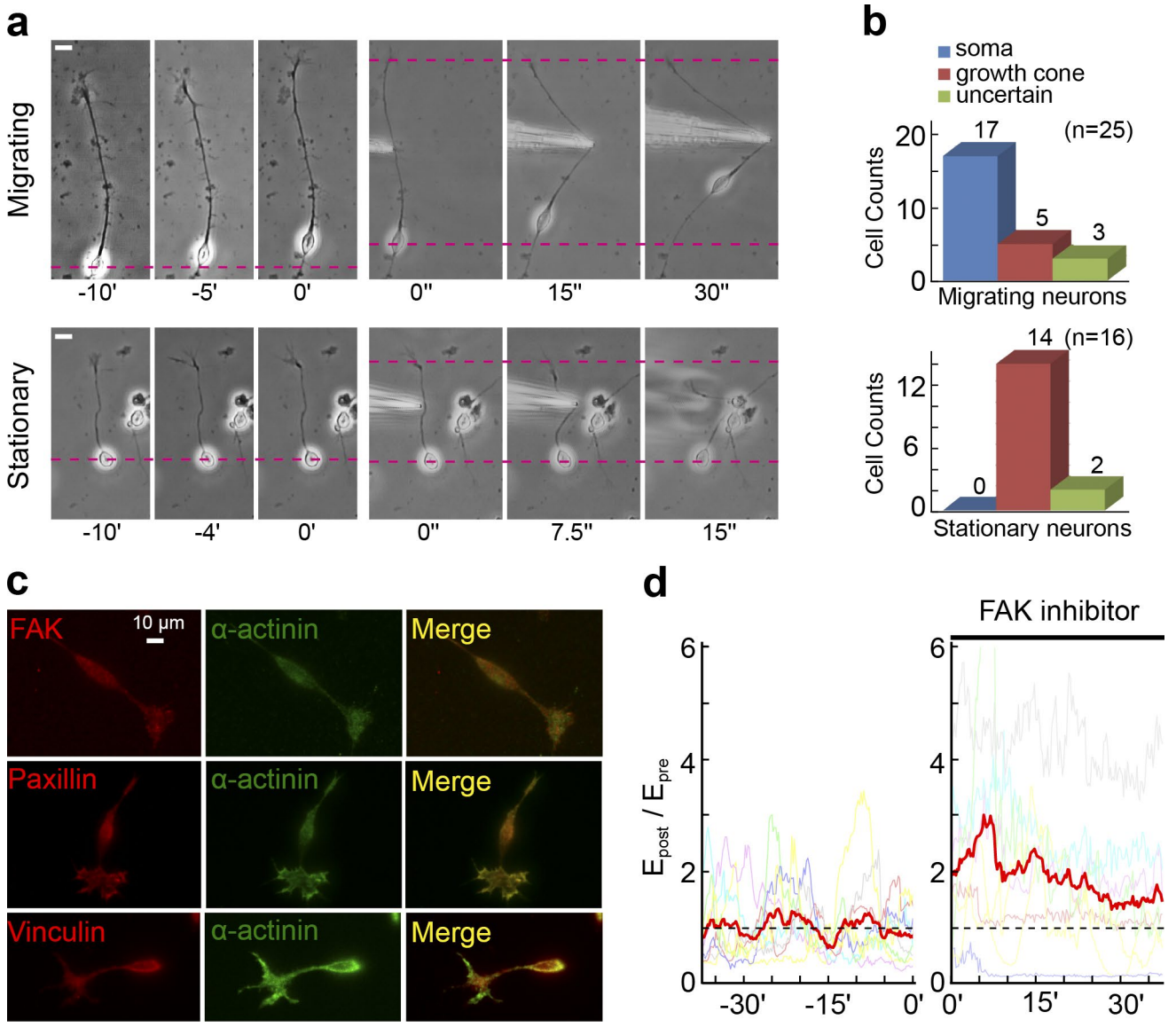

Figure 5. **The role of substrate adhesion in neuronal migration and force generation.** (a) Pulling assay. Pulling the LP of GCs at the middle point. Broken lines show the location of soma and LP growth cone before and after pulling. Bars, 10 µm. (b) Summary of results of the pulling experiments. Under migratory or stationary conditions, the number of GCs that showed the first detachment site at the soma or at the growth cone of LP after pulling is shown. (c) Immunostaining of markers of adhesion complexes (FAK, paxillin, vinculin). (d) FAK inhibition with Y11 (~50–200 µM) enhanced the strain energy of GCs ($n = 7$). Broken lines show the normalized strain energy (1 unit) before drug application.

Kim et al., 2011) and inhibitors (Kim et al., 2011). Conversely, outside-in signaling initiated by extracellular integrin ligands can cause their conformational switch and clustering of integrins, which in turn enhances the adhesion strength (Shattil et al., 2010; Kim et al., 2011).

Cell adhesion can also link many structural and signaling molecules (Plotnikov et al., 2012). For example, as an integrator and biosensor localized in adhesion sites (Mitra et al., 2005), FAK mediates the modulation of Cdc42 by extracellular guidance cues (Matsuda et al., 2012; Myers et al., 2012) and regulates cytoskeletal fluidity, GTPase activity, membrane composition, and the dynamics of focal adhesion, actin, and MTs (Mitra et al., 2005). Adhesion formation and disassembly drives the migration cycle by activating Rho GTPases, which in turn regulate actin polymerization and myosin-II activity, and therefore adhesion dynamics (Parsons et al., 2010).

Physical and chemical components can influence each other reciprocally in an interaction network. Directed actin polymerization brings integrins together to form "nascent" adhesions (Oakes and Gardel, 2014) and increases the membrane tension (Houk et al., 2012). The membrane tension is primarily determined by the mechanical force balance between the cell membrane and traction forces (Lieber et al., 2013) and its increase can activate the myosin contraction (Keren, 2011), but a local increase can inhibit the actin assembly and Rac activation in the distal end (Houk et al., 2012). Myosin-II activity further promotes the polymerization of F-actin (Burridge and Wittchen, 2013; Courtemanche et al., 2013), and the mechanical force exerted on integrins drives focal adhesion growth, protein recruitment, adhesion stabilization, and signal activation (Guilluy et al., 2011; Kuo et al., 2011). In response to mechanical tension, the composition and signaling of substrate adhesion changes,

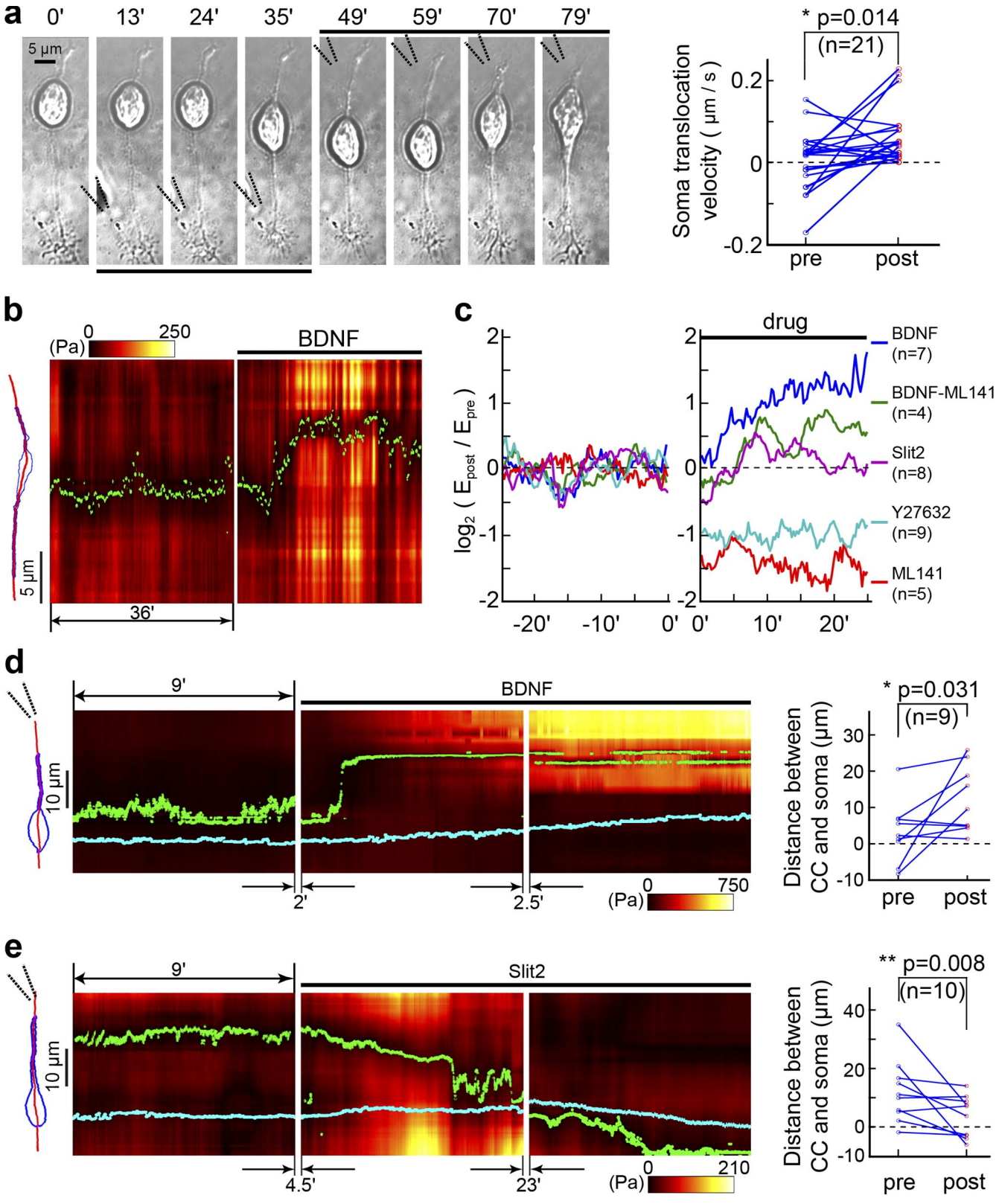

Figure 6. **Guidance cues for neuronal migration regulate activities of CCs.** (a, left) Local perfusion with the attractive cue BDNF (50 ng/ml) guided neuron migration. Broken lines, perfusion pipette for BDNF delivery sequentially at the end of the LP and TP. Note the direction of soma translocation after BDNF perfusion at each location. (a, right) Summary of the BDNF effect on the velocity of soma translocation. BDNF was applied at the distal region of the long process, and the soma velocity (+ and −, toward and away from the long process) was monitored for 9–40 min before and after BDNF application. Note the increase in velocity toward the tip of the LP (P = 0.014, paired *t* test). (b) Line scan (along the red trace shown on the left) of the stress produced by a neuron before and after bath application of BDNF (50 ng/ml), showing overall increase in the stress. Red dots, location of dominant CC. (c) Changes in the total strain energy of the neuron after bath treatment with various agents: BDNF (50 ng/ml) + ML141 (15 μM), Slit2 (0.5 μg/ml), Y27632 (25 μM),

leading either to increased anchorage or controlled disassembly of cell matrix adhesion complexes, both of which are critically involved in cell migration (Wehrle-Haller, 2012).

Fluctuation of traction forces

Fluctuation of traction forces is often observed at subcellular, cellular, and tissue levels, in many cell types and at different stages of developmental processes (Galbraith and Sheetz, 1997; Chan and Odde, 2008; Martin et al., 2009; Trepat et al., 2009; Plotnikov et al., 2012). Such fluctuation helps the cells to sense substrate stiffness (Chan and Odde, 2008; Plotnikov et al., 2012), to align along a special direction (De et al., 2007), and to reshape tissue morphology (Martin et al., 2009). We found that activities of multiple CCs of migratory GCs fluctuate independently during both migratory and stationary phases. The fluctuating CC activities generate apparently random net driving force on the soma, leading to fluctuating soma movement along neurite processes, with the net translocation along the direction of neuronal migration. In analogy to chemotactic migration of *Escherichia coli* (Macnab and Koshland, 1972) and *Caenorhabditis elegans* (Frady et al., 2012), the guidance cues such as BDNF and Slit2 bias the net soma translocation by biasing the apparently random soma translocation through modulation of the relative CC activities at LP and TP.

Regulation of traction forces by BDNF and Slit

Our studies showed that neuronal guidance factors such as BDNF and Slit2 induce GC migration by altering CC activities. Such a mechanism may be generalized to other types of migratory cells. For example, hepatocyte growth factor promotes cell motility and induces strong contractile activity of Madin-Darby canine kidney cells growing on substrates with micropillars (du Roure et al., 2005), and VEGF could enhance the traction force of human umbilical vein endothelial cells by promoting F-actin formation (Yang et al., 2011). The effect of BDNF on traction force may be mediated by cytoplasmic cAMP and the protein kinase A (PKA) activity (Cheng et al., 2011), which then modulate the local activity of Cdc42 (Yuan et al., 2003). However, global modulation of CC activities requires long-range signaling to distant regions of the migrating neuron. The existence of long-range signaling within neuronal cytoplasm is suggested by previous findings that local elevation of cAMP due to BDNF exposure in one neurite may result in cAMP reduction in other neurites of the same neuron (Shelly et al., 2010), and Ca^{2+} elevation due to local exposure to Slit2 at the LP of migrating GCs results in a propagating Ca^{2+} wave to the trailing end of the cell. Such global second messenger signaling is likely to play an important role in the spatiotemporal regulation of CC activities in migrating neurons.

Besides pulling the soma forward, physical forces generated by contact with the environment in the absence of diffusible molecular cues could also bias the direction of cell migration (Theveneau et al., 2010; Weber et al., 2012). The tension on the cell can regulate many signal pathways such as in recruiting myosin-II and regulating its activity (Fernandez-Gonzalez et al., 2009) and regulating gene expression and eventual cell fate (Hiramatsu et al., 2013). Thus, migrating neurons not only passively react to external forces, but also actively influence the mechanical environment for itself and other nearby cells by its active contractile activity and secreted factors. The use of TFM in mapping of traction force generated by migrating cells offers useful means in addressing the interplay between mechanical forces and cellular signaling.

Summary

We have examined the traction force due to neuronal contractility in the presence of cell–substrate adhesion by analyzing cell-induced distortion of the substrate, as revealed by embedded microbeads. While movements of some microbeads could be caused by the cell movement (especially those near the trailing ends of the cell), the cell migration as a whole must result from the action of the net traction force on the entire cell due to asymmetric substrate adhesion at two ends of the cell. This notion is supported by the result of our analysis of the temporal relationship between soma translocation and contractile activity, and by the finding that pharmacological treatments that up- and down-regulate the net traction force produced corresponding changes in soma translocation. This study provides the first comprehensive analysis of the traction force generation by migratory neurons, and suggests an integrated model for the spatiotemporal control of contractile activities in neuronal cytoplasm that reconciles previous findings on force generation in migrating neurons.

Materials and methods

Preparation of PAA gel substrate

The protocol of PAA gel preparation followed a previous report (Wang and Pelham, 1998) with some modifications. In brief, the surface of a glass-bottom culture dish was processed by NaOH (0.1 M, 5 min), (3-Aminopropyl) trimethoxysilane (100%, 3 min), and glutaraldehyde (0.5%, 20 min) to facilitate the covalent attachment of PAA. The PAA gel was prepared by mixing ddH_2O (258 µl), acrylamide (40%, 17 µl), bis-acrylamide (2%, 12 µl), ammonium persulfate (10%, 1.5 µl), and N,N,N',N'-Tetramethylethylenediamine (100%, 0.45 µl), and 15 µl of the mixture was then mixed with 1.4 µl fluorescent microspheres (F8809, F8806; Invitrogen), dropped onto a previously prepared coverglass, and flattened with another cover glass. The dish was then put onto the surface of 24°C water under lamp light for polymerization. 20 min later, the coverglass over the gel was removed and the gel was exposed to UV for activating PAA after adding sulfo-SANPAH solution (1 mM; 22589; Thermo Fisher Scientific). The solution was removed 10 min later, and the gel was washed with Hepes (50 mM) on a shaker for 30 min, three times. The gel-coated dish was used immediately after preparation.

Animals

Newborn Sprague Dawley rats (P0–P2) used in the present study were provided by Shanghai SLAC Laboratory Animal, Inc. Experimental protocols were approved by the Bioethics Committee of the Institute

ML141 (15 µM). Results from all cells examined for five different treatments are shown. (d and e, left) Line scan (red trace on the schematic cell) of the stress produced by two neurons before and after local application of BDNF and Slit2 in front of the long process. Green dots, location of the dominant CC; cyan line, soma center. (d and e, right) Locations of dominant CCs relative to the soma center before and after local perfusion of BDNF and Slit2 for 10–40 min were summarized. Note the forward and rearward movement of the dominant CCs induced by BDNF and Slit2 perfusion at the long process.

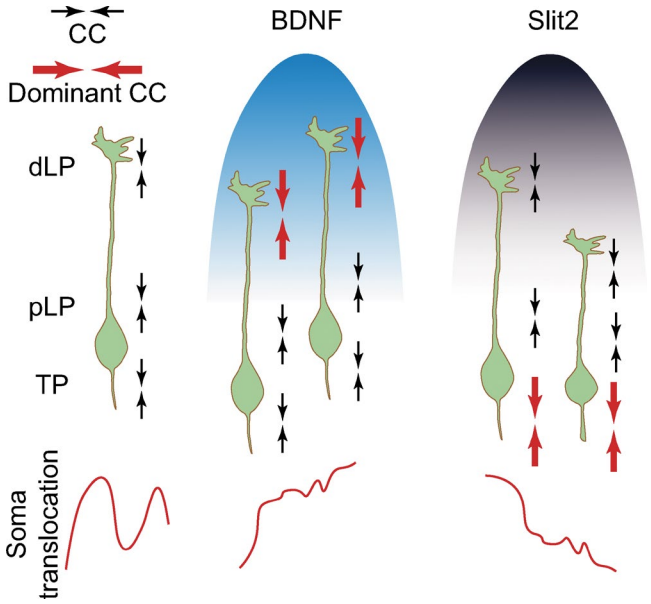

Figure 7. **A model for traction force regulation during neuron migration.** Migratory neurons possess three potential CCs where activated myosin-II generates the traction force. In the absence of guidance cues, contraction activities at the three CCs are weak and fluctuate independently, leading to the stationary state or apparently random fluctuation of soma location. Gradients of guidance cues from the environment bias the relative activities of the three CCs, resulting in preferential net traction toward a specific direction.

of Neuroscience at the Shanghai Institutes for Biological Sciences, Chinese Academy of Sciences.

Cultures of cerebellar GCs

Cultures of dissociated cerebellar GCs were prepared as described previously (Guan et al., 2007) with some modifications. In brief, the cerebellum cortex was dissected on ice from P0–P2 Sprague Dawley rats, digested with 0.125% trypsin (0.25%; Gibco) for 9–11 min at 37°C, and dissociated into single cells by gentle trituration. The PPA gel coverglass was coated with 100 µg/ml poly-D-lysine and 25 µg/ml laminin before cells were plated at a low density (200–300 cells/mm^2) in Neurobasal medium (Invitrogen) supplemented with 10% FBS and 2% B27 (Invitrogen).

Time-lapse imaging and characterization of culture substrate

After 8–10 h of culturing, GCs were placed on a microscope stage for observation. The stage was equipped with a heated incubator to maintain the samples at 5% CO_2 and at 37°C, together with the objective lens (60×, NA 1.4, oil). In local perfusion experiments, the culture medium was changed to prewarmed L-15 (Gibco) without CO_2. Fluorescence images were recorded for 40–240 min at either 0.3 or ∼10–21 s frame interval time using a confocal laser scanning microscope (FV1000; Olympus) with photomultiplier detectors, with 0.103 µm/pixel resolution in bidirectional mode. The acquisition software used was the FV10-ASW program and the pinhole was set to 200 µm to image the beads in the superficial layer of the PAA gel. The fluorochromes of the fluorescent microspheres includes orange (540/560) and crimson (625/645).

After image acquisition, all cells were removed by replacing the culture medium with prewarmed ddH_2O to lyse the cells and to obtain the original locations of the beads before cell attachment. Finally, we performed the stiffness measurement by placing glass balls (200 µm; Polysciences) onto the PAA gel and determining the depth of the pit caused by the glass balls by z-series imaging. The stiffness of the gel was calculated by the Hertzian equation (Chan and Odde, 2008):

$$E = \frac{3(1-\nu^2)f}{4R^{0.5}\delta^{1.5}},$$

where E is Young's modulus (Pa) of the PAA gel, ν is the Poisson ration of the gel ($\nu = 0.3$), R is the radius of the glass ball, δ is depth of the pit, and f is the buoyancy-corrected weight of the glass ball.

The stiffness used in the present study is within the range of 200–400 Pa.

Local perfusion

Local perfusion of pharmacological reagents was performed according to a previous study (Zheng et al., 1994), with some modifications. The drugs were injected into the culture medium by a microinjector (Ultra-MicroPump III; World Precision Instruments, Inc.) with a flow rate of 3–5 nl/min, which produced lower pressure and caused less disturbance to the PAA gel than the Picospritzer (Parker Inc.) used previously. The inner diameter of the micro pipette tip is ∼1–2 µm.

Estimation of deformation, traction force, and strain energy

The microscopic images (12 bit) were transformed into TIF pictures (8 bit) using the Loci plugin (Linkert et al., 2010) for MATLAB, and then aligned and tracked using registration algorithms based on nonlinear optimization (Guizar-Sicairos et al., 2008). All beads were recognized by edge detection and their center locations were determined by the peak of 2D Gaussian fit (Chan and Odde, 2008). The displacement of the bead center was determined as the peak location for the cross correlation between the images before and after cell lysis (over a bead-centered square window of ∼80 × 80 pixels; Butler et al., 2002). The bead displacement map was transformed into traction force map and the strain energy was calculated by Fourier transform traction cytometry (FTTC; Butler et al., 2002). Simply, the Boussinesq solution,

$$u_i = \sum_{j=1}^{m} K(r_{ij})F_j,$$

(where K is green function, u is the strain of the gel, and F is the traction force in the gel) is Fourier transformed (FT) into a simple multiplication,

$$\tilde{u}(k) = \tilde{K}(k)\tilde{F}(k),$$

where $\tilde{u}$, $\tilde{K}$, and $\tilde{F}$ are the Fourier transform of each parameter; and k is the wave vectors). Then the stress can be calculated by

$$F = FT_2^{-1}(\tilde{K}^{-1}\tilde{u}),$$

where FT_2^{-1} is the two dimensional inverse Fourier transform. The kernel $\tilde{K}$ is

$$\tilde{K}\left(k\right) = \frac{1+\nu}{E}\frac{2}{k^3}\begin{bmatrix}(1-\nu)k^2+\nu k_y^2 & \nu k_x k_y \\ \nu k_x k_y & (1-\nu)k^2+\nu k_y^2\end{bmatrix},$$

where E is Young's modulus of the PAA gel, $k = \sqrt{k_x^2+k_y^2}$, and ν indicates the Poisson ration of the gel ($\nu = 0.3$).

The total strain energy of a neuron was calculated by summing the energy density around the neuron.

2D interpolation

2D scattered displacement vectors were interpolated by the MATLAB scatteredInterpolant class. The vector components x and y were interpolated, respectively, and then joined together.

Determination of the location of dominant CC

We first determined the direction of traction forces at all pixels along the neuron axis and then identified the CC location as the region where

near-neighbor pixels exhibited the maximal change in the direction of the traction force (Δangle).

Immunostaining

Neurons were fixed with 4% paraformaldehyde (in PBS) for 20 min at room temperature and then incubated with 0.25% Triton X-100 (in PBS) and 1% BSA (in PBS) for 1 h for permeabilization and blocking. Primary antibodies (FAK [pTyr397] antibody, 700255, Invitrogen; Paxillin [pY118] antibody, 44722G, Invitrogen; anti-vinculin antibody, V9264, Sigma-Aldrich; Phospho-Myosin Light Chain 2 [Ser19] Mouse mAb, 3657, Cell Signaling Technology; anti-green fluorescent protein, A11120, Molecular Probes) were added with corresponding blocking solution and incubated overnight at 4°C. Corresponding secondary antibodies and DAPI were added and incubated for 2 h at room temperature.

TIRF microscopy

After transfected with recombinant vector (GFP–α-actinin) and 8–10 h of culturing, GCs were immunostained with primary antibodies of FAK, paxillin, vinculin, and GFP and then with secondary antibodies. The prepared samples were imaged with an inverted microscope (Ti-E; Nikon) at room temperature. The setup was equipped with an Apochromat TIRF oil-immersion objective lens (60×, NA 1.49), together with a camera (DU-897 X-4696; Andor) with a resolution of 0.27 µm/pix. The imaging software was NIS-Element and fluorochromes were Alexa Fluor 488 and Alexa Fluor 546.

Online supplemental material

Fig. S1 shows that CCs can also be visualized by a 3D color map of stress magnitude and pinwheel color map of stress directions. Each process of the GC with multiple primary neurites can generate its own CC. Fig. S2 shows more cases of stress dynamics analysis by the line scan of the stress maps along GC axis and distribution of dominant CCs for 18 cells. Fig. S3 shows more cases of asymmetric stress maps during soma translocation. Fig. S4 shows that there are typical focal adhesions and stress fibers in glial cells but not in GCs, and that the traction force generated by glia cells is much larger than that of GCs. Table S1 shows the numbers of GCs with one, two, or three CCs in all the GCs we examined. Video 1 shows the spatiotemporal dynamics of the stress generated by a migrating GC during a 30-min period. Online supplemental material is available at http://www.jcb.org/cgi/content/full/jcb.201410068/DC1. Additional data are available in the JCB DataViewer at http://dx.doi.org/10.1083/jcb.201410068.dv.

Acknowledgements

We thank Dr. David J. Odde of University of Minnesota for kindly sharing the program codes for microbead recognition.

This work was supported by grants from Ministry of Science and Technology (973 Program, 2011CBA00400) and the Chinese Academy of Sciences (Strategic Priority Research Program, XDB02020001).

The authors declare no competing financial interests.

Submitted: 20 October 2014
Accepted: 27 April 2015

References

Akhshi, T.K., D. Wernike, and A. Piekny. 2014. Microtubules and actin crosstalk in cell migration and division. *Cytoskeleton (Hoboken).* 71:1–23. http://dx.doi.org/10.1002/cm.21150

Ayala, R., T. Shu, and L.H. Tsai. 2007. Trekking across the brain: the journey of neuronal migration. *Cell.* 128:29–43. http://dx.doi.org/10.1016/j.cell.2006.12.021

Balaban, N.Q., U.S. Schwarz, D. Riveline, P. Goichberg, G. Tzur, I. Sabanay, D. Mahalu, S. Safran, A. Bershadsky, L. Addadi, and B. Geiger. 2001. Force and focal adhesion assembly: a close relationship studied using elastic micropatterned substrates. *Nat. Cell Biol.* 3:466–472. http://dx.doi.org/10.1038/35074532

Behrndt, M., G. Salbreux, P. Campinho, R. Hauschild, F. Oswald, J. Roensch, S.W. Grill, and C.P. Heisenberg. 2012. Forces driving epithelial spreading in zebrafish gastrulation. *Science.* 338:257–260. http://dx.doi.org/10.1126/science.1224143

Borghesani, P.R., J.M. Peyrin, R. Klein, J. Rubin, A.R. Carter, P.M. Schwartz, A. Luster, G. Corfas, and R.A. Segal. 2002. BDNF stimulates migration of cerebellar granule cells. *Development.* 129:1435–1442.

Brangwynne, C.P., F.C. MacKintosh, S. Kumar, N.A. Geisse, J. Talbot, L. Mahadevan, K.K. Parker, D.E. Ingber, and D.A. Weitz. 2006. Microtubules can bear enhanced compressive loads in living cells because of lateral reinforcement. *J. Cell Biol.* 173:733–741. http://dx.doi.org/10.1083/jcb.200601060

Brugués, A., E. Anon, V. Conte, J.H. Veldhuis, M. Gupta, J. Colombelli, J.J. Munoz, G.W. Brodland, B. Ladoux, and X. Trepat. 2014. Forces driving epithelial wound healing. *Nat. Phys.* 10:683–690. http://dx.doi.org/10.1038/nphys3040

Burridge, K., and E.S. Wittchen. 2013. The tension mounts: stress fibers as force-generating mechanotransducers. *J. Cell Biol.* 200:9–19.

Butler, J.P., I.M. Tolić-Nørrelykke, B. Fabry, and J.J. Fredberg. 2002. Traction fields, moments, and strain energy that cells exert on their surroundings. *Am. J. Physiol. Cell Physiol.* 282:C595–C605. http://dx.doi.org/10.1152/ajpcell.00270.2001

Carlier, M.F., A. Ducruix, and D. Pantaloni. 1999. Signalling to actin: the Cdc42-N-WASP-Arp2/3 connection. *Chem. Biol.* 6:R235–R240. http://dx.doi.org/10.1016/S1074-5521(99)80107-0

Chan, C.E., and D.J. Odde. 2008. Traction dynamics of filopodia on compliant substrates. *Science.* 322:1687–1691. http://dx.doi.org/10.1126/science.1163595

Cheng, P.L., H. Lu, M. Shelly, H. Gao, and M.M. Poo. 2011. Phosphorylation of E3 ligase Smurf1 switches its substrate preference in support of axon development. *Neuron.* 69:231–243. http://dx.doi.org/10.1016/j.neuron.2010.12.021

Courtemanche, N., J.Y. Lee, T.D. Pollard, and E.C. Greene. 2013. Tension modulates actin filament polymerization mediated by formin and profilin. *Proc. Natl. Acad. Sci. USA.* 110:9752–9757. http://dx.doi.org/10.1073/pnas.1308257110

De, R., A. Zemel, and S.A. Safran. 2007. Dynamics of cell orientation. *Nat. Phys.* 3:655–659. http://dx.doi.org/10.1038/nphys680

Dogterom, M., J.W. Kerssemakers, G. Romet-Lemonne, and M.E. Janson. 2005. Force generation by dynamic microtubules. *Curr. Opin. Cell Biol.* 17:67–74. http://dx.doi.org/10.1016/j.ceb.2004.12.011

du Roure, O., A. Saez, A. Buguin, R.H. Austin, P. Chavrier, P. Silberzan, and B. Ladoux. 2005. Force mapping in epithelial cell migration. *Proc. Natl. Acad. Sci. USA.* 102:2390–2395. (published erratum appears in *Proc. Natl. Acad. Sci. USA.* 102:14122) http://dx.doi.org/10.1073/pnas.0408482102

Even-Ram, S., A.D. Doyle, M.A. Conti, K. Matsumoto, R.S. Adelstein, and K.M. Yamada. 2007. Myosin IIA regulates cell motility and actomyosin-microtubule crosstalk. *Nat. Cell Biol.* 9:299–309. http://dx.doi.org/10.1038/ncb1540

Falnikar, A., S. Tole, and P.W. Baas. 2011. Kinesin-5, a mitotic microtubule-associated motor protein, modulates neuronal migration. *Mol. Biol. Cell.* 22:1561–1574. http://dx.doi.org/10.1091/mbc.E10-11-0905

Feng, Y., and C.A. Walsh. 2001. Protein-protein interactions, cytoskeletal regulation and neuronal migration. *Nat. Rev. Neurosci.* 2:408–416. http://dx.doi.org/10.1038/35077559

Fernandez-Gonzalez, R., S.M. Simoes, J.C. Röper, S. Eaton, and J.A. Zallen. 2009. Myosin II dynamics are regulated by tension in intercalating cells. *Dev. Cell.* 17:736–743. http://dx.doi.org/10.1016/j.devcel.2009.09.003

Frady, E.P., C.R. Palmer, and W.B. Kristan Jr. 2012. Sexual attraction: sex-specific wiring of neural circuitry. *Curr. Biol.* 22:R953–R956. http://dx.doi.org/10.1016/j.cub.2012.10.003

Galbraith, C.G., and M.P. Sheetz. 1997. A micromachined device provides a new bend on fibroblast traction forces. *Proc. Natl. Acad. Sci. USA.* 94:9114–9118. http://dx.doi.org/10.1073/pnas.94.17.9114

Gardel, M.L., B. Sabass, L. Ji, G. Danuser, U.S. Schwarz, and C.M. Waterman. 2008. Traction stress in focal adhesions correlates biphasically with actin retrograde flow speed. *J. Cell Biol.* 183:999–1005. http://dx.doi.org/10.1083/jcb.200810060

Golubovskaya, V.M., S. Figel, B.T. Ho, C.P. Johnson, M. Yemma, G. Huang, M. Zheng, C. Nyberg, A. Magis, D.A. Ostrov, et al. 2012. A small molecule focal adhesion kinase (FAK) inhibitor, targeting Y397 site: 1-(2-hydroxyethyl)-3, 5, 7-triaza-1-azoniatricyclo [3.3.1.1(3,7)]decane; bromide effectively inhibits FAK autophosphorylation activity and decreases cancer cell viability, clonogenicity and tumor growth in vivo. *Carcinogenesis.* 33:1004–1013. http://dx.doi.org/10.1093/carcin/bgs120

Gomes, E.R., S. Jani, and G.G. Gundersen. 2005. Nuclear movement regulated by Cdc42, MRCK, myosin, and actin flow establishes MTOC polarization in migrating cells. *Cell.* 121:451–463. http://dx.doi.org/10.1016/j.cell.2005.02.022

Grashoff, C., B.D. Hoffman, M.D. Brenner, R. Zhou, M. Parsons, M.T. Yang, M.A. McLean, S.G. Sligar, C.S. Chen, T. Ha, and M.A. Schwartz. 2010. Measuring mechanical tension across vinculin reveals regulation of focal adhesion dynamics. *Nature.* 466:263–266. http://dx.doi.org/10.1038/nature09198

Guan, C.B., H.T. Xu, M. Jin, X.B. Yuan, and M.M. Poo. 2007. Long-range Ca^{2+} signaling from growth cone to soma mediates reversal of neuronal migration induced by slit-2. *Cell.* 129:385–395. http://dx.doi.org/10.1016/j.cell.2007.01.051

Guilluy, C., V. Swaminathan, R. Garcia-Mata, E.T. O'Brien, R. Superfine, and K. Burridge. 2011. The Rho GEFs LARG and GEF-H1 regulate the mechanical response to force on integrins. *Nat. Cell Biol.* 13:722–727. http://dx.doi.org/10.1038/ncb2254

Guizar-Sicairos, M., S.T. Thurman, and J.R. Fienup. 2008. Efficient subpixel image registration algorithms. *Opt. Lett.* 33:156–158. http://dx.doi.org/10.1364/OL.33.000156

Guo, W.H., and Y.L. Wang. 2012. A three-component mechanism for fibroblast migration with a contractile cell body that couples a myosin II-independent propulsive anterior to a myosin II-dependent resistive tail. *Mol. Biol. Cell.* 23:1657–1663. http://dx.doi.org/10.1091/mbc.E11-06-0556

Hatten, M.E. 1999. Central nervous system neuronal migration. *Annu. Rev. Neurosci.* 22:511–539. http://dx.doi.org/10.1146/annurev.neuro.22.1.511

He, M., Z.H. Zhang, C.B. Guan, D. Xia, and X.B. Yuan. 2010. Leading tip drives soma translocation via forward F-actin flow during neuronal migration. *J. Neurosci.* 30:10885–10898. http://dx.doi.org/10.1523/JNEUROSCI.0240-10.2010

Hiramatsu, R., T. Matsuoka, C. Kimura-Yoshida, S.W. Han, K. Mochida, T. Adachi, S. Takayama, and I. Matsuo. 2013. External mechanical cues trigger the establishment of the anterior-posterior axis in early mouse embryos. *Dev. Cell.* 27:131–144. http://dx.doi.org/10.1016/j.devcel.2013.09.026

Houk, A.R., A. Jilkine, C.O. Mejean, R. Boltyanskiy, E.R. Dufresne, S.B. Angenent, S.J. Altschuler, L.F. Wu, and O.D. Weiner. 2012. Membrane tension maintains cell polarity by confining signals to the leading edge during neutrophil migration. *Cell.* 148:175–188. http://dx.doi.org/10.1016/j.cell.2011.10.050

Kaverina, I., and A. Straube. 2011. Regulation of cell migration by dynamic microtubules. *Semin. Cell Dev. Biol.* 22:968–974. http://dx.doi.org/10.1016/j.semcdb.2011.09.017

Kaverina, I., K. Rottner, and J.V. Small. 1998. Targeting, capture, and stabilization of microtubules at early focal adhesions. *J. Cell Biol.* 142:181–190. http://dx.doi.org/10.1083/jcb.142.1.181

Keren, K. 2011. Membrane tension leads the way. *Proc. Natl. Acad. Sci. USA.* 108:14379–14380. http://dx.doi.org/10.1073/pnas.1111671108

Kim, C., F. Ye, and M.H. Ginsberg. 2011. Regulation of integrin activation. *Annu. Rev. Cell Dev. Biol.* 27:321–345. http://dx.doi.org/10.1146/annurev-cellbio-100109-104104

Kimura, K., M. Ito, M. Amano, K. Chihara, Y. Fukata, M. Nakafuku, B. Yamamori, J. Feng, T. Nakano, K. Okawa, et al. 1996. Regulation of myosin phosphatase by Rho and Rho-associated kinase (Rho-kinase). *Science.* 273:245–248. http://dx.doi.org/10.1126/science.273.5272.245

Kuo, J.C., X. Han, C.T. Hsiao, J.R. Yates III, and C.M. Waterman. 2011. Analysis of the myosin-II-responsive focal adhesion proteome reveals a role for β-Pix in negative regulation of focal adhesion maturation. *Nat. Cell Biol.* 13:383–393. http://dx.doi.org/10.1038/ncb2216

Lieber, A.D., S. Yehudai-Resheff, E.L. Barnhart, J.A. Theriot, and K. Keren. 2013. Membrane tension in rapidly moving cells is determined by cytoskeletal forces. *Curr. Biol.* 23:1409–1417. http://dx.doi.org/10.1016/j.cub.2013.05.063

Linkert, M., C.T. Rueden, C. Allan, J.M. Burel, W. Moore, A. Patterson, B. Loranger, J. Moore, C. Neves, D. Macdonald, et al. 2010. Metadata matters: access to image data in the real world. *J. Cell Biol.* 189:777–782. http://dx.doi.org/10.1083/jcb.201004104

Macnab, R.M., and D.E. Koshland Jr. 1972. The gradient-sensing mechanism in bacterial chemotaxis. *Proc. Natl. Acad. Sci. USA.* 69:2509–2512. http://dx.doi.org/10.1073/pnas.69.9.2509

Martin, A.C., M. Kaschube, and E.F. Wieschaus. 2009. Pulsed contractions of an actin-myosin network drive apical constriction. *Nature.* 457:495–499. http://dx.doi.org/10.1038/nature07522

Martini, F.J., and M. Valdeolmillos. 2010. Actomyosin contraction at the cell rear drives nuclear translocation in migrating cortical interneurons. *J. Neurosci.* 30:8660–8670. http://dx.doi.org/10.1523/JNEUROSCI.1962-10.2010

Matsuda, S., T. Fujita, M. Kajiya, K. Takeda, H. Shiba, H. Kawaguchi, and H. Kurihara. 2012. Brain-derived neurotrophic factor induces migration of endothelial cells through a TrkB-ERK-integrin αVβ3-FAK cascade. *J. Cell. Physiol.* 227:2123–2129. http://dx.doi.org/10.1002/jcp.22942

Mitra, S.K., D.A. Hanson, and D.D. Schlaepfer. 2005. Focal adhesion kinase: in command and control of cell motility. *Nat. Rev. Mol. Cell Biol.* 6:56–68. http://dx.doi.org/10.1038/nrm1549

Moore, S.W., and M.P. Sheetz. 2011. Biophysics of substrate interaction: influence on neural motility, differentiation, and repair. *Dev. Neurobiol.* 71:1090–1101. http://dx.doi.org/10.1002/dneu.20947

Munevar, S., Y. Wang, and M. Dembo. 2001. Traction force microscopy of migrating normal and H-ras transformed 3T3 fibroblasts. *Biophys. J.* 80:1744–1757. http://dx.doi.org/10.1016/S0006-3495(01)76145-0

Myers, J.P., and T.M. Gomez. 2011. Focal adhesion kinase promotes integrin adhesion dynamics necessary for chemotropic turning of nerve growth cones. *J. Neurosci.* 31:13585–13595. http://dx.doi.org/10.1523/JNEUROSCI.2381-11.2011

Myers, J.P., E. Robles, A. Ducharme-Smith, and T.M. Gomez. 2012. Focal adhesion kinase modulates Cdc42 activity downstream of positive and negative axon guidance cues. *J. Cell Sci.* 125:2918–2929. http://dx.doi.org/10.1242/jcs.100107

Oakes, P.W., and M.L. Gardel. 2014. Stressing the limits of focal adhesion mechanosensitivity. *Curr. Opin. Cell Biol.* 30:68–73. http://dx.doi.org/10.1016/j.ceb.2014.06.003

Palazzo, A.F., C.H. Eng, D.D. Schlaepfer, E.E. Marcantonio, and G.G. Gundersen. 2004. Localized stabilization of microtubules by integrin- and FAK-facilitated Rho signaling. *Science.* 303:836–839. http://dx.doi.org/10.1126/science.1091325

Park, H., and M.M. Poo. 2013. Neurotrophin regulation of neural circuit development and function. *Nat. Rev. Neurosci.* 14:7–23. http://dx.doi.org/10.1038/nrn3379

Parsons, J.T., A.R. Horwitz, and M.A. Schwartz. 2010. Cell adhesion: integrating cytoskeletal dynamics and cellular tension. *Nat. Rev. Mol. Cell Biol.* 11:633–643. http://dx.doi.org/10.1038/nrm2957

Patla, I., T. Volberg, N. Elad, V. Hirschfeld-Warneken, C. Grashoff, R. Fässler, J.P. Spatz, B. Geiger, and O. Medalia. 2010. Dissecting the molecular architecture of integrin adhesion sites by cryo-electron tomography. *Nat. Cell Biol.* 12:909–915. http://dx.doi.org/10.1038/ncb2095

Plotnikov, S.V., A.M. Pasapera, B. Sabass, and C.M. Waterman. 2012. Force fluctuations within focal adhesions mediate ECM-rigidity sensing to guide directed cell migration. *Cell.* 151:1513–1527. http://dx.doi.org/10.1016/j.cell.2012.11.034

Poblete-Naredo, I., A.M. Guillem, C. Juárez, R.C. Zepeda, L. Ramírez, M. Caba, L.C. Hernández-Kelly, J. Aguilera, E. López-Bayghen, and A. Ortega. 2011. Brain-derived neurotrophic factor and its receptors in Bergmann glia cells. *Neurochem. Int.* 59:1133–1144. http://dx.doi.org/10.1016/j.neuint.2011.10.002

Rape, A., W.H. Guo, and Y.L. Wang. 2011. Microtubule depolymerization induces traction force increase through two distinct pathways. *J. Cell Sci.* 124:4233–4240. http://dx.doi.org/10.1242/jcs.090563

Roca-Cusachs, P., A. del Rio, E. Puklin-Faucher, N.C. Gauthier, N. Biais, and M.P. Sheetz. 2013. Integrin-dependent force transmission to the extracellular matrix by α-actinin triggers adhesion maturation. *Proc. Natl. Acad. Sci. USA.* 110:E1361–E1370. http://dx.doi.org/10.1073/pnas.1220723110

Salbreux, G., G. Charras, and E. Paluch. 2012. Actin cortex mechanics and cellular morphogenesis. *Trends Cell Biol.* 22:536–545. http://dx.doi.org/10.1016/j.tcb.2012.07.001

Serra-Picamal, X., V. Conte, R. Vincent, E. Anon, D.T. Tambe, E. Bazellieres, J.P. Butler, J.J. Fredberg, and X. Trepat. 2012. Mechanical waves during tissue expansion. *Nat. Phys.* 8:628–634. http://dx.doi.org/10.1038/nphys2355

Shattil, S.J., C. Kim, and M.H. Ginsberg. 2010. The final steps of integrin activation: the end game. *Nat. Rev. Mol. Cell Biol.* 11:288–300. http://dx.doi.org/10.1038/nrm2871

Shelly, M., B.K. Lim, L. Cancedda, S.C. Heilshorn, H. Gao, and M.M. Poo. 2010. Local and long-range reciprocal regulation of cAMP and cGMP in axon/dendrite formation. *Science.* 327:547–552. http://dx.doi.org/10.1126/science.1179735

Sieg, D.J., C.R. Hauck, D. Ilic, C.K. Klingbeil, E. Schaefer, C.H. Damsky, and D.D. Schlaepfer. 2000. FAK integrates growth-factor and integrin sig-

nals to promote cell migration. *Nat. Cell Biol.* 2:249–256. http://dx.doi.org/10.1038/35010517

Solecki, D.J., N. Trivedi, E.-E. Govek, R.A. Kerekes, S.S. Gleason, and M.E. Hatten. 2009. Myosin II motors and F-actin dynamics drive the coordinated movement of the centrosome and soma during CNS glial-guided neuronal migration. *Neuron.* 63:63–80. http://dx.doi.org/10.1016/j.neuron.2009.05.028

Spedden, E., J.D. White, E.N. Naumova, D.L. Kaplan, and C. Staii. 2012. Elasticity maps of living neurons measured by combined fluorescence and atomic force microscopy. *Biophys. J.* 103:868–877. http://dx.doi.org/10.1016/j.bpj.2012.08.005

Theveneau, E., L. Marchant, S. Kuriyama, M. Gull, B. Moepps, M. Parsons, and R. Mayor. 2010. Collective chemotaxis requires contact-dependent cell polarity. *Dev. Cell.* 19:39–53. http://dx.doi.org/10.1016/j.devcel.2010.06.012

Trepat, X., M.R. Wasserman, T.E. Angelini, E. Millet, D.A. Weitz, J.P. Butler, and J.J. Fredberg. 2009. Physical forces during collective cell migration. *Nat. Phys.* 5:426–430. http://dx.doi.org/10.1038/nphys1269

Tsai, J.W., K.H. Bremner, and R.B. Vallee. 2007. Dual subcellular roles for LIS1 and dynein in radial neuronal migration in live brain tissue. *Nat. Neurosci.* 10:970–979. http://dx.doi.org/10.1038/nn1934

Vicente-Manzanares, M., X. Ma, R.S. Adelstein, and A.R. Horwitz. 2009. Non-muscle myosin II takes centre stage in cell adhesion and migration. *Nat. Rev. Mol. Cell Biol.* 10:778–790. http://dx.doi.org/10.1038/nrm2786

Wang, Y.-L., and R.J. Pelham Jr. 1998. Preparation of a flexible, porous polyacrylamide substrate for mechanical studies of cultured cells. *Methods Enzymol.* 298:489–496. http://dx.doi.org/10.1016/S0076-6879(98)98041-7

Waterman-Storer, C.M., and E. Salmon. 1999. Positive feedback interactions between microtubule and actin dynamics during cell motility. *Curr. Opin. Cell Biol.* 11:61–67. http://dx.doi.org/10.1016/S0955-0674(99)80008-8

Webb, D.J., K. Donais, L.A. Whitmore, S.M. Thomas, C.E. Turner, J.T. Parsons, and A.F. Horwitz. 2004. FAK-Src signalling through paxillin, ERK and MLCK regulates adhesion disassembly. *Nat. Cell Biol.* 6:154–161. http://dx.doi.org/10.1038/ncb1094

Weber, G.F., M.A. Bjerke, and D.W. DeSimone. 2012. A mechanoresponsive cadherin-keratin complex directs polarized protrusive behavior and collective cell migration. *Dev. Cell.* 22:104–115. http://dx.doi.org/10.1016/j.devcel.2011.10.013

Wehrle-Haller, B. 2012. Assembly and disassembly of cell matrix adhesions. *Curr. Opin. Cell Biol.* 24:569–581. http://dx.doi.org/10.1016/j.ceb.2012.06.010

Wilkinson, S., H.F. Paterson, and C.J. Marshall. 2005. Cdc42-MRCK and Rho-ROCK signalling cooperate in myosin phosphorylation and cell invasion. *Nat. Cell Biol.* 7:255–261. http://dx.doi.org/10.1038/ncb1230

Woo, S., and T.M. Gomez. 2006. Rac1 and RhoA promote neurite outgrowth through formation and stabilization of growth cone point contacts. *J. Neurosci.* 26:1418–1428. http://dx.doi.org/10.1523/JNEUROSCI.4209-05.2006

Wu, W., K. Wong, J. Chen, Z. Jiang, S. Dupuis, J.Y. Wu, and Y. Rao. 1999. Directional guidance of neuronal migration in the olfactory system by the protein Slit. *Nature.* 400:331–336. http://dx.doi.org/10.1038/22477

Xiao, H., P. Verdier-Pinard, N. Fernandez-Fuentes, B. Burd, R. Angeletti, A. Fiser, S.B. Horwitz, and G.A. Orr. 2006. Insights into the mechanism of microtubule stabilization by Taxol. *Proc. Natl. Acad. Sci. USA.* 103:10166–10173. http://dx.doi.org/10.1073/pnas.0603704103

Yang, M.T., D.H. Reich, and C.S. Chen. 2011. Measurement and analysis of traction force dynamics in response to vasoactive agonists. *Integr. Biol. (Camb).* 3:663–674. http://dx.doi.org/10.1039/c0ib00156b

Yim, E.K., and M.P. Sheetz. 2012. Force-dependent cell signaling in stem cell differentiation. *Stem Cell Res. Ther.* 3:41. http://dx.doi.org/10.1186/scrt132

Yuan, X.B., M. Jin, X. Xu, Y.Q. Song, C.P. Wu, M.M. Poo, and S. Duan. 2003. Signalling and crosstalk of Rho GTPases in mediating axon guidance. *Nat. Cell Biol.* 5:38–45. http://dx.doi.org/10.1038/ncb895

Zheng, J.Q., Z. Zheng, and M. Poo. 1994. Long-range signaling in growing neurons after local elevation of cyclic AMP-dependent activity. *J. Cell Biol.* 127:1693–1701. http://dx.doi.org/10.1083/jcb.127.6.1693